

Numerical studies of the value of including pupil intensity information in multi-frame blind deconvolution calculations for data measured in the presence of scintillation

Michael C. Roggemann¹, Paul A. Billings², Jeffery Houchard³

¹Pacific Defense Solutions, Kihei, HI, and Michigan Technological University, Houghton, MI

²Textron Corporation, Kihei, HI

³Pacific Defense Solutions, Kihei, HI

Abstract

Under most situations where it is appropriate to reconstruct imagery using a multi-frame blind deconvolution (MFBD) algorithm, defects in the point spread function (PSF) are dominated by phase errors arising from atmospheric turbulence. However, under extreme conditions, such as horizontal imaging or imaging at low elevation angles, scintillation can also arise. These amplitude errors also contribute to the degradation of the PSF. MFBD algorithms which parameterize the phase aberrations in the pupil generally neglect pupil intensity information. The key issue addressed in this paper is whether incorporating information about the pupil intensity in an MFBD algorithm improves the accuracy of the reconstruction. Using a numerical simulation approach to address this issue, we show that incorporating pupil intensity information improves the quality of the reconstructed images only slightly.

Introduction

Atmospheric turbulence affects the density, and hence, the index of refraction of air [Goodman, 1985]. As a result, many combinations of turbulence strength and path length give rise to turbulence-induced wave front errors that are dominated by phase effects. Turbulence-induced phase errors can turn into amplitude errors through wave propagation when the combination of turbulence-induced phase error strength and propagation path are sufficient [Beland, 1993]. Under these conditions the instantaneous point spread function (PSF) of the imaging system/atmosphere combination is affected by both phase and amplitude errors. For an aperture larger than a few times the Fried seeing parameter r_0 , the instantaneous PSFs arising under these conditions are badly speckled, and individual images of space objects measured with short exposures are generally unintelligible.

A number of strategies have been developed to overcome turbulence effects on imaging systems. At the present time, they span a spectrum of hardware and software complexity and expense. Historically, post detection image processing

algorithms (referred to as speckle imaging techniques) were developed as the first means of overcoming turbulence effects in imaging systems [Roggemann, 1996]. These techniques exploit the fact that certain specialized second and third order moments of the Fourier transform of short exposure images contain high spatial frequency information about the object. Under a reasonable range of practical conditions, this information can be measured with sufficient signal-to-noise ratio (SNR) to be used for restoration. Due to the placement of optical SSA assets atop mountains, reasonably good seeing is often realized, and scintillation effects are generally negligible in actual practice. It should be noted that speckle imaging techniques do not explicitly estimate the aberrations or PSF associated with any particular image measurement.

More recently, multi-frame blind deconvolution (MFBD) techniques were developed to overcome turbulence effects in image reconstruction. MFBD algorithms exploit the fact that the object associated with a sequence of short exposure measured images can be considered constant, while the atmosphere continuously changes. Combining this observation with maximum-likelihood estimation formalism yields feasible algorithms. MFBD algorithms jointly estimate both the common object and various atmospheric descriptions (either the PSFs or the wavefront aberrations) associated with each measured image. Two broad classes of algorithms have been developed – one based on the expectation-maximization algorithm [Schulz, 1993] and the other based on a fully parameterized joint estimation of the object and the aberration [Billings, 2001]. It should be noted that these two algorithms have much in common, and they differ primarily in their approach to optimizing and regularizing the same log-likelihood function.

To address a need for corrections performed in real-time, adaptive optical (AO) systems have been developed to correct turbulence-induced aberrations while images are being measured. AO systems require complicated and expensive hardware: a tilt measurement and control system, a wave front sensor (WFS), a deformable mirror (DM), a closed loop controller linking the WFS to the DM in a manner which insures stability, very high speed, multi-channel electronics, and an additional set of optical surfaces which reduce the radiometric throughput of the system. In spite of the expense and complexity, a large number of AO systems exist today, and the design and implementation of systems with a reasonable number of DM degrees-of-freedom (i.e., several tens to a few hundred) has been reduced to an engineering exercise. We also note that a number of hybrid techniques combining elements of AO and post detection processing have been developed [Roggemann, 1996].

The success of the techniques mentioned above in overcoming turbulence effects has led to considerable research interest in “extending the envelope” of operation. A key underlying assumption in the development of speckle imaging, MFBD, and AO is that the underlying turbulence process is “weak”. In other words, the turbulence-induced errors are dominated by phase effects, and amplitude fluctuations are negligible. If the propagation path is sufficiently long,

or if the turbulence is sufficiently strong, wave propagation mechanics cause amplitude fluctuations to arise, which are referred to as scintillation [Beland, 1993]. Amplitude fluctuations are generally ignored in MFBD processing and in the control loop of AO systems. One direction of research is to examine the effects of relaxing the assumption of weak turbulence, exploring avenues for incorporating information about the amplitude fluctuations if it is available, and evaluating the performance of the resulting algorithm. Situations where scintillation could be non-negligible include horizontal path imaging near the surface of the Earth and high zenith-angle imaging of space objects. In addition to scintillation, strong turbulence can cause light emanating from even closely spaced points on the object to propagate through a significantly different volume of turbulence, giving rise to a condition called anisoplanatism. Under anisoplanatic imaging conditions no single PSF can accurately model the blur in the image, and in fact, the PSF is a space-varying function [Beland, 1993]. Anisoplanatism effects will also be strong under most practical combinations of observation geometries and turbulence strengths for the horizontal path scenario.

In this paper we explore the implications of incorporating pupil intensity measurements into a specific implementation of an MFBD algorithm [Billings, 2001] and evaluate performance. To create scintillated fields falling in the pupil we developed a wave optics simulation of incoherent, horizontal path imaging. We presumed that a separate system was available to measure the pupil intensity fluctuations, and we incorporated this data into the MFBD processing. We compared these results to those of the baseline MFBD code, which ignores intensity fluctuations and assumes a uniform intensity pupil field. We find that these two approaches provide object estimates which have comparable mean squared errors (MSE) compared to the known input object. However, the aberration parameter estimates for the two cases are significantly different. We conjecture that when pupil intensity fluctuations are ignored, the variations in the PSFs due to the amplitude fluctuations are encoded in small perturbations of the aberration coefficients.

The remainder of the paper is organized as follows. In the next section we briefly review the relevant theoretical considerations, specifically, the mathematical description of the concept of weak turbulence, the MFBD algorithm, and our means of incorporating pupil intensity information. In the following section we present the details of the wave optics simulation used to create the data sets processed. We then present the results of our study. The final section presents our conclusions.

Theory

The implementation of MFBD that we are working with is based on Ref. [Billings, 2001]. We summarize this technique here, but without the details of the derivation. We are working with shot noise limited images in the present case. The noise-free image model for the k^{th} image of a set of turbulence corrupted images is obtained from Fourier optics [Goodman, 2005] as

$$(1) \quad g_k(x_i) = \sum_{x_o} f(x_o) h_k(x_i - x_o),$$

where x_o is a 2-D coordinate in object space, x_i is a 2-D coordinate in image space, $f(x_o)$ is the object, and $h_k(x_i, x_o)$ is the k^{th} PSF. The photo-electron count statistics of photon-limited images are governed by Poisson statistics. The appropriate log-likelihood function is [Paxman, 1992; Schulz, 1993]

$$(2) \quad L_P(f, h) = \sum_k \sum_{x_i} d_k(x_i) \ln[g_k(x_i)] - g_k(x_i),$$

where $d_k(x_i)$ is the k^{th} realization of the Poisson noise-corrupted image, and the notation $L_P(f, h)$ indicates that the log-likelihood function depends upon both the object estimate f and the set of PSFs $\{h_k\}$. The goal of maximum likelihood estimation is then to maximize $L_P(f, h)$ by appropriate choices for the object $f(x_o)$ and PSFs $\{h_k\}$. It is common to parameterize the PSFs in terms of the phase aberration by describing the phase aberration as a combination of a basis set of functions in the pupil of the telescope [Paxman, 1992; Schulz, 1993], and this approach is taken here by parameterizing the aberration in terms of the first 91 Zernike polynomials [Roggemann, 1996]. A standard and widely used multidimensional optimizer is used to maximize the log-likelihood function given in Eq. (2) over all points in the object estimate and the 91 Zernike polynomial coefficient estimates associated with each measured image. Excellent results have been obtained using this approach over a wide range of conditions.

Fluctuations of the amplitude of the field falling on the pupil directly affect the PSFs, $\{h_k\}$. Let the instantaneous complex field falling on the pupil be represented by

$$(3) \quad U_P(x_P) = A(x_P) e^{j\varphi_P(x_P)},$$

where x_P is a coordinate in the pupil plane, $A(x_P)$ represents the amplitude of the field, and $\varphi_P(x_P)$ is the phase of the field.

The instantaneous PSF is related to $U_P(x_P)$ by

$$(4) \quad h_k(x_I) = \left| FT\{U_P(x_P)\} \right|_{f_I = x_I / \lambda f_l}^2,$$

where $FT\{\bullet\}$ represents the 2-D Fourier transform operator, f_I is the independent frequency space variable arising from the Fourier transform operation, f_l is the focal length of the imaging systems, λ is the mean

wavelength, and the subscript $f_I = x_I / \lambda f_l$ indicates the mapping between the spatial frequency variable f_I and the physical location in the image plane x_I .

In the MFBD algorithm implemented for this study [Billings, 2001], and others [Schulz, 1993; Paxman, 1992], the estimated turbulence-induced phase error $\tilde{\varphi}_P(x_P)$ is modeled as a linear combination of Zernike polynomials

$$(5) \quad \tilde{\varphi}_P(x_P) = \sum_{n=1}^{N_Z} a_n Z_n(x_P),$$

where $Z_n(x_P)$ represents the n^{th} Zernike polynomial as ordered by Noll [Roggemann, 1996], a_n represents the weight associated with the n^{th} Zernike polynomial, and N_Z represents the number of Zernike polynomials used in the estimation process. The object intensities are estimated directly. Hence, the optimization algorithm has $N_P^2 + KN_Z$ free parameters. The optimizer is based on a widely used multidimensional optimization technique [Billings, 2001], which requires analytic gradients to operate most efficiently. The required gradients, which are the partial derivatives of the log-likelihood function with respect to both the pixel intensity estimates and the Zernike polynomial weights, were derived in [Paxman, 1992].

The baseline algorithm ignores the possibility of amplitude fluctuations in the field falling on the pupil. As a result, the baseline algorithm models fluctuations in the PSF due to non-uniform $A(x_P)$ by adjusting the a_n 's. Our modification to the baseline algorithm provides the ability to use information about the intensity of the field falling on the pupil $|A(x_P)|^2$ assuming it can be measured. This pupil amplitude information is selectively enabled or disabled under user control to test and compare the importance of providing this typically "missing" information to the MFBD algorithm. When enabled, the known truth of the pupil intensity from our wave-optics simulation is provided to the part of the MFBD algorithm which estimates the PSFs. As a result, when enabled, we expect that the MFBD estimated a_n 's will be different when there is scintillation present as compared to the baseline algorithm which assumes a constant pupil amplitude.

The key question addressed in this study is whether incorporating pupil intensity data in the MFBD calculations yields results which are in some sense better than ignoring the pupil intensity fluctuations in the presence of scintillation. We evaluate the answer to this question by computing and comparing the sum of the squared difference between the estimated object and the real object for each case. Addressing these issues requires a wave optics simulation be used to create the simulated data. We now describe such a simulation.

Simulation

The simulation developed for this application is a wave optics simulation of imaging over a horizontal path. The combination of turbulence strength and path length was chosen to cause significant scintillation in the field arriving at the pupil. Our goal was to implement an incoherent imaging simulation of a spoke target, while isolating the effects of scintillation from the effects of anisoplanatism. This is feasible in simulation, although not in actual practice. Our approach to this problem was as follows. A wave optics propagator based on the angular spectrum was used to propagate light emanating from an on-axis point source in the target plane to the pupil. The light falling on the pupil was scintillated, and was used to form a PSF, which was then convolved with the test object to form an isoplanatic image. This process was repeated to form a data set of 100 images which were then used as input to the MFB processing. To further isolate the effects of scintillation on the process, the images were simulated at a very high light level. We now present the details of the inputs to the simulation.

Figure 1 shows the input object. It is a spoke target widely used to measure resolution. In object space it is 25 cm in diameter, viewed at a range of 1 km, at a mean wavelength of 700 nm, with a 30 cm diameter aperture. It should be noted that these conditions give rise to anisoplanatic effects, as the object subtends 250 μ Rad, while the isoplanatic angle is on the order of 10 μ Rad for the cases run here. The actual C_n^2 profiles used to generate the results are presented in the results section. It should be noted that in actual practice, when imaging anisoplanatic objects, measuring the pupil field would be of little practical value since the scintillation patterns from object points separated by significantly more than the isoplanatic angle would arrive superimposed at the pupil, and “sorting” these contributions would be at least impractical and likely impossible. Hence, while we conducted this investigation for a horizontal path, it is our expectation that the real-world impact of the results shown below will be for imaging satellites, which are generally isoplanatic, under conditions where scintillation could be significant, such as at low elevation angles.

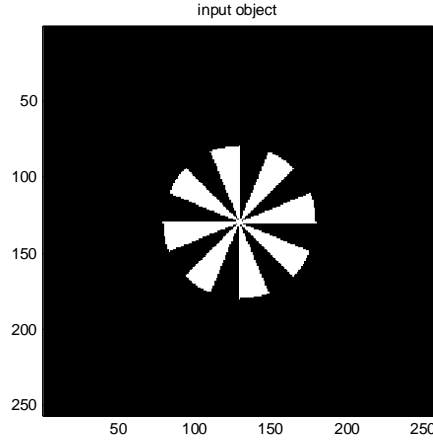


Figure 1. Input object for horizontal imaging simulations.

The imagery generated was Nyquist sampled. The array size used to hold both the pupil and the object was $N_P = 256$. The diameter of the circular pupil spanned $N_P/2$ samples, and the sample spacing was $\Delta x = 2.34$ mm. The angular sample spacing in both image and object space is given by

$$(6) \quad \Delta\theta = \frac{\lambda}{N\Delta x},$$

which evaluates to $\Delta\theta = 1.17 \mu\text{Rad}$. The sampling requirement for the angular spectrum propagator used here is

$$(7) \quad N_P \geq \frac{2\lambda z}{\Delta x^2},$$

where $z = 1$ km is the path length. In the present case the right hand side of Eq. (7) evaluates to 256, so the sampling requirement for the propagator is satisfied.

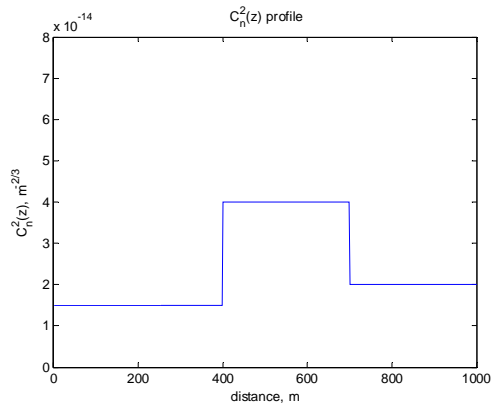
A layered turbulence model which had 10 layers was used. The phase screen generator requires the plane wave Fried parameter r_0 as input for each layer. The values of r_0 for each layer were calculated by starting at the object and integrating toward the pupil an appropriate distance. Phase screens were equally spaced, with the first screen encountered by the light placed 100 m from the object, and the last screen placed in the telescope pupil. Photon-limited images were simulated with a mean number of photon events per image equal to 10^6 . Noise free pupil intensity information was extracted from the simulation and used to compute the MFBD image reconstructions for the cases where pupil intensity information was used. We now present the results of our study.

Results

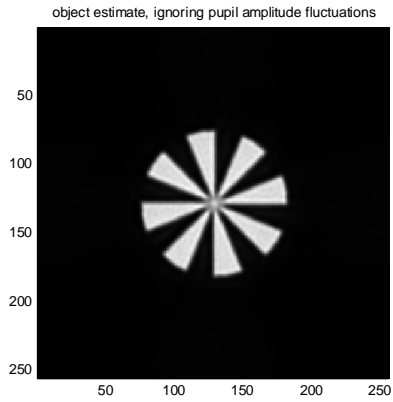
Figures 2, 3, and 4 show the results of applying the MFBD algorithm with and without including the pupil intensity information in the reconstruction. Also shown are the input C_n^2 profiles for each case, the resulting standard atmospheric optics parameters, and the sum of the square of the differences between the object estimates and the true object, represented by ε^2 (the true object and the estimated object are normalized to unit energy). The log amplitude variance $\sigma_\chi^2 = 0.32$ for the case presented in Fig. 2 is at the edge of saturated scintillation, and the values of σ_χ^2 for the data used to prepare Figs. 3 and 4 are past the threshold of saturated intensity fluctuations.

Inspection of Figs. 2, 3, and 4 shows that there is very little subjective difference in the quality of the reconstructed images regardless of whether pupil intensity information is used in the reconstruction – even in the case of very strong scintillation. The use of pupil intensity information resulted in reconstructions with a lower sum squared error metric ε^2 for the strong scintillation cases shown in Figs. 3 and 4 but not for the weaker case shown in Fig. 2.

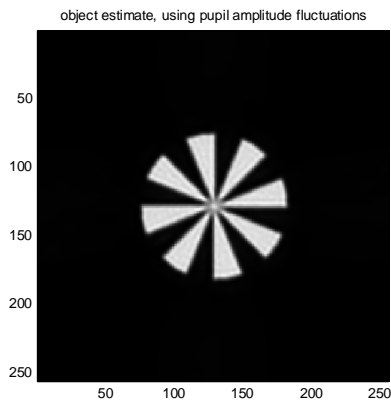
Perhaps more interesting, is comparing the values for the estimated Zernike polynomial coefficients obtained with and without the use of the pupil intensity information. Example results are presented in Fig. 5, where the estimated coefficients for one image (drawn from the data used to make Fig. 3) are presented for the cases of using and not using pupil intensity information in the MFBD image reconstruction. The results in Fig. 5 are representative of the results obtained for the rest of this data set. Inspection of Fig. 5 shows that when pupil intensity information is used in the process, significantly different values are estimated for the Zernike polynomial coefficients than when pupil intensity information is not used. It should be noted that due to the nature of wave propagation mechanics the phase arriving at the pupil is “wrapped” in the sense that only the principal value of the phase is available without some sort of unwrapping [Ghiglia, 1998], and there may also be branch cuts in the phase map [Fried, 1998]. As a result, simply projecting the incident phase onto the Zernike polynomial basis set would yield misleading results. In this case the true values of the Zernike polynomial coefficients associated with the field falling on the pupil are not available, and are not displayed in Fig. 5.



(a)



(b)



(c)

$$r_0^{\text{pln}} = 1.79 \text{ cm}$$

$$r_0^{\text{sph}} = 3.53 \text{ cm}$$

$$\theta_0 = 9.8 \text{ } \mu\text{Rad}$$

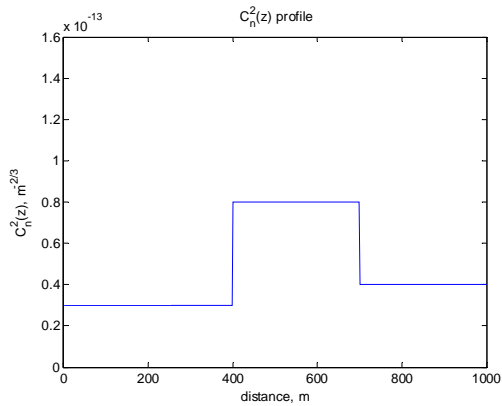
$$\sigma_\chi^2 = 0.32$$

$$\varepsilon^2(\text{no intensity}) = 3.7284\text{e-}005$$

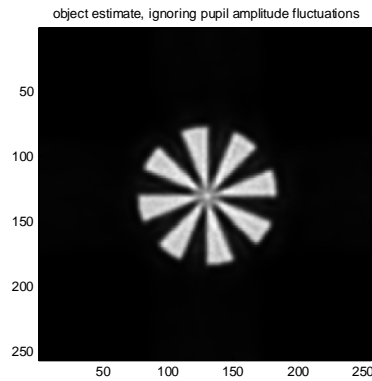
$$\varepsilon^2(\text{with intensity}) = 3.9676\text{e-}005$$

(d)

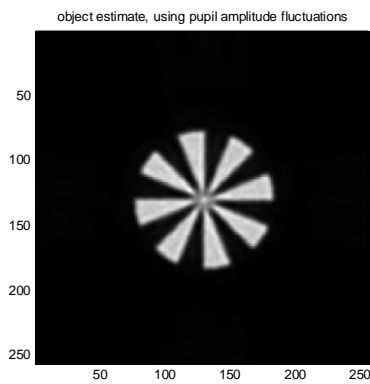
Figure 2. Example outputs of the simulation runs: (a) input C_n^2 profile; (b) object estimate obtained ignoring amplitude fluctuations in the pupil; (c) object estimate obtained using the “measured” pupil intensity; (d) parameter values for this case.



(a)



(b)



(c)

$$r_0^{\text{pln}} = 1.18 \text{ cm}$$

$$r_0^{\text{sph}} = 2.33 \text{ cm}$$

$$\theta_0 = 6.4 \text{ } \mu\text{Rad}$$

$$\sigma_\chi^2 = 0.65$$

$$\varepsilon^2(\text{no intensity}) = 4.8577\text{e-}005$$

$$\varepsilon^2(\text{with intensity}) = 4.3956\text{e-}005$$

(d)

Figure 3. Example outputs of the simulation runs: (a) input C_n^2 profile; (b) object estimate obtained ignoring amplitude fluctuations in the pupil; (c) object estimate obtained using the “measured” pupil intensity; (d) parameter values for this case.

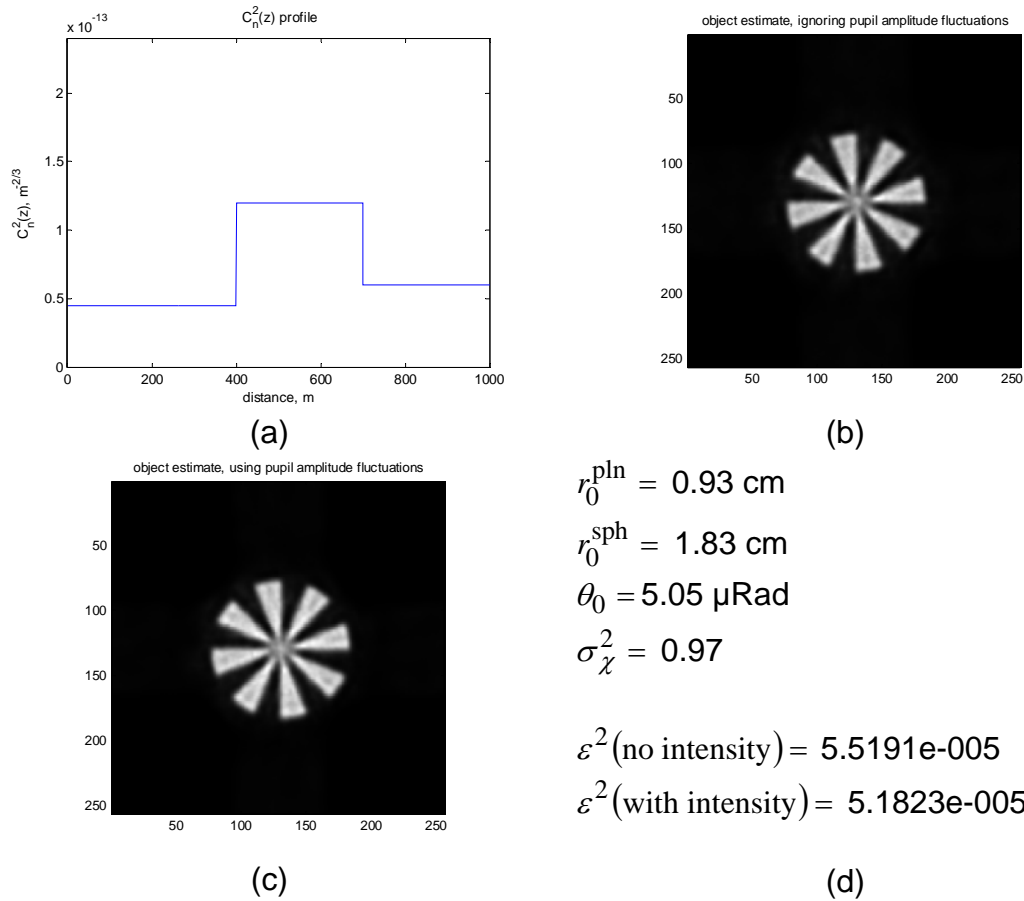


Figure 4. Example outputs of the simulation runs: (a) input C_n^2 profile; (b) object estimate obtained ignoring amplitude fluctuations in the pupil; (c) object estimate obtained using the “measured” pupil intensity; (d) parameter values for this case.

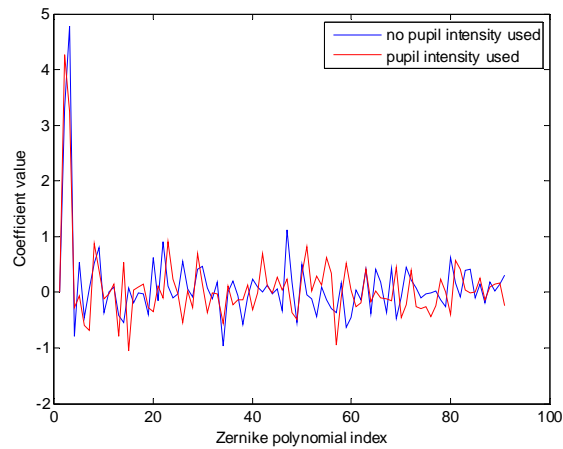


Figure 5. Example of Zernike polynomial coefficients estimated both with and without pupil intensity information.

Conclusion

We have presented a study of the value of incorporating scintillation information into the MFBD image reconstruction process. A wave optics simulation was used to create the data sets processed, and minor modifications were made to an existing MFBD code to incorporate pupil intensity information into the PSF estimation process. Since the subjective image quality does not vary significantly when pupil intensity information is used compared to the case when this information is not used, we conjecture that good PSFs must result in both cases. There are, however, significant differences in the estimated Zernike coefficients.

References

[Beland, 1993] Beland, R. R., "Propagation through atmospheric optical turbulence", *IR/EO Handbook, Vol. 2*, F. G. Smith, Ed., SPIE Press, Bellingham, WA, 1993.

[Billings, 2001] Billings, P. A., M. F. Reiley, and B. E. Stribling, "Mitigating turbulence-induced image blur using multiframe blind deconvolution", AMOS Technical Conference, Wailea, HI, p506-512, Sept., 2001.

[Fried, 1998] Fried, D. L., "Branch point problem in adaptive optics", *J. Opt. Soc. Am. A*, vol. 15, p2759-2768, 1998.

[Ghiglia, 1998] Ghiglia, D. C., and M. D. Pritt, *Two-Dimensional Phase Unwrapping: Theory, Algorithms, and Software*, Wiley Inter-Science, New York, 1998.

[Goodman, 1985] Goodman, J. W., *Statistical Optics*, Wiley-Interscience, New York, 1985.

[Goodman, 2005] Goodman, J. W., *Introduction to Fourier Optics, 3rd Edition*, Roberts & Company Publishers, Greenwood Village, CO, 2005.

[Paxman, 1992] Paxman, R. G., T. J. Schulz, and J. R. Feinup, "Joint estimation of object and aberrations by using phase diversity", *J. Opt. Soc. Am. A*, vol. 9, p1072-1085, 1992.

[Roggemann, 1996] Roggemann, M. C., and B. M. Welsh, *Imaging Through Turbulence*, CRC Press, Boca Raton, FL, 1996.

[Roggemann, 1998] Roggemann, M. C., and T. J. Schulz, "Algorithm to increase the largest aberration that can be reconstructed from Hartmann sensor measurements," *Appl. Opt.* 37, 4321-4329, 1998.

[Schulz, 1993] Schulz, T. J., "Multiframe blind deconvolution of astronomical images", *J. Opt. Soc. Am. A*, vol. 10, p1064-1073, 1993.